Effective Design Principles for Leakless Strand Displacement Systems

Supporting Information

Boya Wang[1], Chris Thachuk[2], Andrew D. Ellington[3], Erik Winfree[2,4,5], and David Soloveichik[1,*]

[1] *Electrical and Computer Engineering, University of Texas at Austin, Austin, TX 78712, USA*
[2] *Computer Science, California Institute of Technology, Pasadena, CA 91125, USA*
[3] *Department of Chemistry and Biochemistry, Institute for Cellular and Molecular Biology, University of Texas at Austin, Austin, TX 78712, USA*
[4] *Computation and Neural Systems, California Institute of Technology, Pasadena, CA 91125, USA*
[5] *Bioengineering, California Institute of Technology, Pasadena, CA 91125, USA*

*To whom correspondence should be addressed; E-mail: david.soloveichik@utexas.edu

Contents

www.pnas.org/cgi/doi/10.1073/pnas.1806859115

S1 Materials and Methods

S1.1 Sequence design

For all experiments other than testing the sequence generality of the DLD design (Figure S1), and the *OR* circuit, we used the following procedure to generate the DNA sequences. The sequence space of a translator or translator cascade can be represented by a single contiguous sequence (i.e. $x_1x_2y_1y_2$ for the SLD and DLD designs). This contiguous sequence can then be mapped to the corresponding domains and their complements. First the sequence candidates were generated randomly from a three letter alphabet (equal probability of A, T, C). The ATC alphabet was used for all the top strands (and naturally the complementary ATG alphabet for the bottom strands) in order to minimize self-complementarity of a strand (no possibility to form strong C-G bonds) [1, 2]. Then the candidates were selected if they passed the following tests:

1. To avoid synthesis errors, no more than 4 of the same nucleotide in a row, and no more than 7 A/T's in a row;
2. To ensure toeholds are sufficiently strong, toeholds are 5 nt long with 2 C's;
3. To reduce spurious binding between DNA strands, the frequency of C is limited: every double-stranded region has 30% to 37% C's;
4. To minimize fraying, the last two nucleotides in double-stranded regions must contain exactly one C.

Among all the candidate sequences, we chose the sequence with the minimal length of the longest repeated segments. Mathematica code written to generate sequences according to these criteria is available upon request.

For the sequence generality experiment (Figure S1) the sequence of each long domain (15 nt) was picked independently from the Seesaw circuit pool [3].

For the *OR* circuit, the neighboring domains are not unique (i.e. z_{21} is both adjacent to x_{52} and x_{62} domains on the 5' end), and thus one contiguous sequence could not represent the sequence space, while preserving adjacency. Therefore we generated the individual signal sequences one after another: The signal sequences (30 nt) for the input x_1, intermediate output y_1, intermediate output z_1 and final output w_1 were the sequences from the linear DLD translator cascade. Other signal sequences were generated and selected one by one. To find a specific signal sequence, first a pool of 30 nt sequence candidates was generated randomly (three letter alphabet, as above). Then candidates were eliminated if they did not pass tests (1)-(4) listed above. Finally, we computed the maximal common substring between the candidate sequence and each already-selected signal sequences. The sequence candidate with the shortest maximal common substring was selected.

Note that clamps may increase the reversibility of the desired reaction by creating a short toehold for the backward reaction (see Figure 1c of the main text). Since input strands do not contribute to leak (triggering is desired), we extended the input strand X by two nucleotides for the SLD and DLD single translator schemes to ensure an irreversible reaction with *F1*.

S1.2 Materials and Methods

S1.2.1 DNA oligonucleotides

DNA oligos were synthesized by Integrated DNA Technologies (IDT). The unlabeled oligos were ordered PAGE purified by IDT, while the fluorophore and quencher-labeled oligos were ordered HPLC (high-performance liquid chromatography) purified by IDT. Upon arrival, these DNA oligonucleotides were suspended in Milli-Q water. The concentration of each strand was quantified by NanoDrop. The absorbance at 260 nm was recorded and the concentration (c) was calculated as $c = [\text{Absorbance}]/e$, where e is the extinction coefficient provided by IDT. Usually, the nominal stock concentration for single-stranded DNA was $\sim$100 μM.

S1.2.2 Fuel formation

The buffer for all experiments was TAE/Mg^{2+} buffer (0.04 M Tris, 1 mM EDTA, 12.5 mM Mg^{2+}, pH balanced to 8.0 by acetate). DNA fuel duplexes were formed through annealing after mixing strands for each duplex with nominally correct stochiometry at 40 μM. The annealing process was performed in a PCR thermocycler: incubating DNA strands at 95 ℃ for 5 minutes and then slowly cooling down with the rate 0.1 ℃/s to 20 ℃.

S1.2.3 Fuel purification

All the fuel complexes were PAGE purified after annealing. PAGE purification was used to remove single-stranded DNA or poorly formed complexes. 12% native PAGE gels of 1.5 mm thickness were made by mixing 15 mL 40% acrylamide/bis, 5 mL 10$\times$ TAE/Mg^{2+} buffer and Milli-Q water to 50 mL, then adding 200 μL 10% APS and 50 μL TEMED to help polymerization. 10% glycerol was mixed with complexes to weigh down DNA samples in the loading lanes. Purification gels were run at 160 V for $\sim$5 hours, cooled by a fan. The 1$\times$ TAE/Mg^{2+} running buffer was refreshed every 2 hours. The proper bands visualized under UV light were cut from the gels and eluted as follows. The cut-out gel bands were crushed into small pieces and soaked in 1$\times$ TAE/Mg^{2+} solution for at least 48 hours at 25 ℃. Afterward, the elution solution was centrifuged at $>$16,000$\times g$ for 15 min and the upper part of the liquid was retained.

The concentration for complexes was calculated as $c = \textit{Absorbance}/e$. We calculated the extinction coefficient e for a complex by adding up the extinction coefficents of its single-stranded and double-stranded parts, computed separately. We calculated single-stranded extinction coefficients according to the parameters in ref. [4], and used the methods of ref. [5] to estimate the extinction coefficient of double-helical DNA from the extinction coefficients of its two strands. For high concentration experiments (the concentrations for fuel species more than 2 μM) and translator cascade/circuit experiments, a further step was needed to increase the stock concentration of purified complexes: 500 μL of purified complexes were transferred to centrifugal filters (Amicon Ultra-0.5 mL, 10K device) and centrifuged at $>$16,000$\times g$ for 30 min. The concentrated sample was then collected and its concentration quantified as above. Usually 20 μL of concentrated sample with the concentration factor $\sim$25$\times$ could be collected.

S1.2.4 Reporter formation

Quantifying the concentration of multi-stranded complexes is relatively inaccurate because of errors in estimating extinction coefficients. Since accurate quantitation of reporters ensures a better normalization of fluorescence data, the annealed reporters were not PAGE purified, thus avoiding duplex concentration quantitation. We annealed reporter complexes with 20% excess of top strand (labeled by quencher), which was meant to ensure the formation of reporter complexes without leaving free fluorophore labeled bottom strands contributing to the background signal. As the reporter top strands do not have a toehold domain, we expect reporter top strands to be inert with respect to our translators and translator cascades.

S1.3 Kinetic experiments

Kinetic experiments for the *OR* circuit were measured on a BioTech Cytation 5 multi-mode reader. All the other kinetic experiments were performed using a Tecan M200 Plate Reader. The low volume NBS (non-binding surface) 384 well plates with clear flat bottom were used, purchased from Corning corporation (# 3544). The sample volume was chosen to be 18 μL, which resulted in a good signal-to-noise ratio, while minimizing total DNA (i.e., experiment cost). Sealing tapes were attached to the surface of plates to avoid evaporation during multi-hour experiments. For experiments using the FAM fluorophore, the excitation wavelength was 485 nm and the emission wavelength was 520 nm. For experiments using the ROX fluorophore, the excitation wavelength was 577 nm and the emission wavelength was 608 nm. Throughout, the excitation bandwidth was fixed at 9 nm and the emission bandwidth was fixed at 20 nm. Fluorescence was measured from the bottom to reduce the noise caused by the small droplets condensed on the sealing tape. Integration time was 20 μs, and data points were taken every minute. To test that no photo-bleaching occurs in the experimental setting, the signal of a fluorophore labeled single strand was tested and it was stable ($\pm 1\%$) over the 10 hour experiment duration. Variation between different wells was within $\pm 2\%$. All the samples were mixed and prepared at room temperature (close to 25 ℃). For the experiments conducted at 25 ℃, the time interval between fully mixing the samples (fuels plus any input) and starting measurement was within 3 minutes. For the experiments conducted at higher than 25 ℃, other than the time interval for mixing samples, the plate was incubated in the plate reader for another 10 minutes prior to data collection to let the samples reach the same temperature as the experimental setting. Time 0 on kinetic plots represents the moment the first data point was measured.

S1.4 Fluorescence data normalization

A calibration curve was used to convert arbitrary fluorescence units to the corresponding signal concentration. We obtained different calibration curves for each temperature as follows. The reporter was titrated with a strand that can fully trigger the reporter (separate the fluorophore and quencher) at different concentrations (up to 100 nM). The background fluorescence signal (untriggered reporter) was set to be the baseline and subtracted from all the other data. The calibration curve was made through a linear fit of the titrated fluorescence signal and the concentration of the triggering strand (the R-squared value is usually above 0.98).

All the experimental results except for the triggering signal of the TLD translator (Figure S9) and the *OR* circuit in the main text (Figure 9b) were normalized by their corresponding calibration

curves as follows. First, the background fluorescence resulting from untriggered reporter was subtracted from all data traces. (Since background fluorescence intensity depended upon the total amount of reporter, we obtained different background curves for different reporter concentrations.) Then, all data traces were divided by the slope (fluorescence signal per nM) of the calibration curve.

High concentration desired triggering experiments (TLD translator, Figure S9) were normalized by an internal control because the fluorescence signal far exceeded the bounds of the reporter calibration curve. The internal control was conducted by triggering the TLD reporter directly by the output strand Y with the same concentration as the input X of the translator. The fluorescence signal per nM was calculated by dividing the fluorescence signal by the concentration of the triggering strand. Normalization then involved subtracting the background signal of the untriggered reporter, and dividing by the fluorescence signal per nM calculated above.

The *OR* circuit outputs 1 when the reporter was fully triggered (Figure 9b). Since the reporter is limiting, output 1 corresponds to the highest triggering signal. Thus, to normalize the data, the first data point of the leak signal was subtracted, since it was taken to be the background for all wells. Then the signals were divided by the highest fluorescence value among the triggering signals of different wells. In this way, the value of the first data point of the leak signal is set to 0 and the highest triggering signal is set to 1.

S1.5 PAGE visualization

Native PAGE was run to verify the products of the translators of the different designs. 12% native PAGE gels were prepared as described in **Section S1.2.3**. The samples containing only one species (fuels or inputs) were directly loaded. The samples containing more than one species were incubated for 2 hours before being loaded. The concentration of each species was 200 nM. The gels were run at 150 V for 4 hours.

All the gels were first directly scanned by BioRad ChemiDoc MP imaging system without staining, so that the property of self fluorescence of each sample could be recorded. Since the fluorophore was ROX with the excitation and emission wavelength of 588 nm and 608 nm respectively, the excitation source was the green epi-illuminator and a 605/50 filter was used. Afterward, the gels were stained with Sybr Gold for 10 min and scanned by the imager. The excitation source was the UV illuminator and a standard SybrGold filter was used.

The relative leak intensities were calculated as the ratio of the intensity of the given band divided by the intensity of the triggered band (where the reporter is triggered by the input signal). The background intensity of the gel was subtracted from both the measured intensity of the target band and the triggered band.

S1.6 Data fitting

The rate constants of the DLD leak model (Table S1) were fitted to the kinetics of the DLD leak (Figure 6b in the main text) using the “FindMinimum” function in Mathematica to minimize the logarithm of the mean squared error between the proposed model and the experimental data of DLD leak kinetics in Figure 6b. The error between the data and the model simulation was

calculated as

$$Error = \log\left(\frac{1}{n}\sum_{t\in \textit{traces}}(\textit{data(t)} - \textit{model(t)})^2\right)$$

where *data(t)* is the concentration experimentally measured and normalized at time t, and *model(t)* is the concentration calculated by the ODE model at time t, and n is the total number of data points.

The free parameters in the model for data fitting were the logarithms of the rate constants k_1, k_{-1}, k_2, k_{-2}, k_3, k_{-3}. To accommodate initial leak, the kinetic curves were set to have different concentration offsets (the concentrations at time 0) as additional free parameters. For the model shown in Table 1, the offsets for the 4 different kinetic curves were 15 nM (1 μM), 18 nM (2 μM), 35 nM (5 μM) and 32 nM (10 μM).

S2 The sequence generality of the DLD design

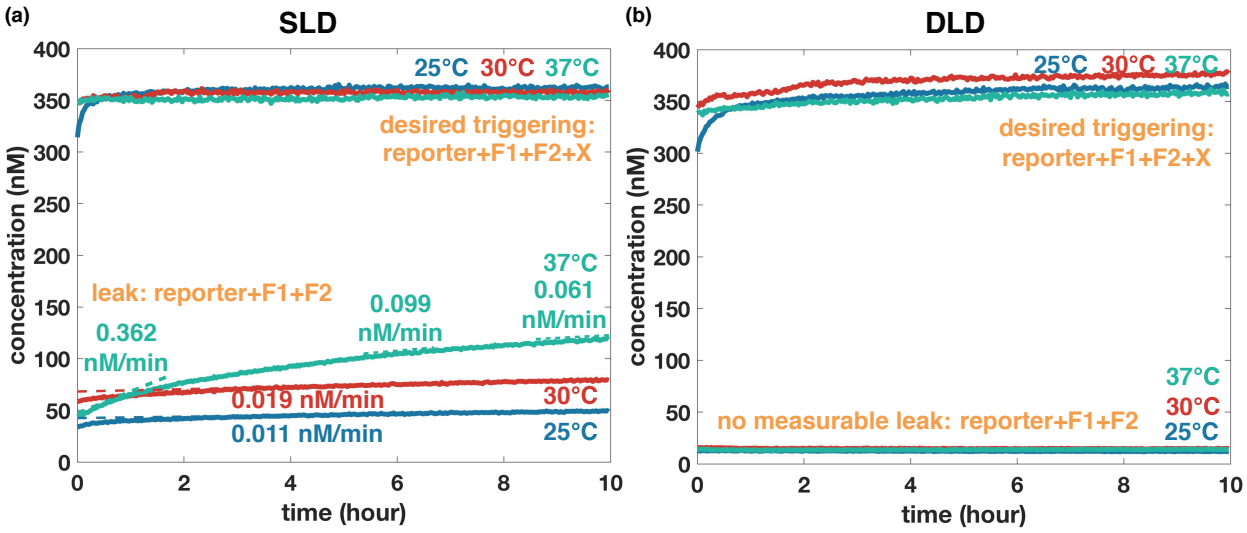

Figure S1: The sequence generality experiment comparing the kinetics of (a) the SLD translator and (b) the DLD translator with and without input X. The sequences used for these experiments were picked from the Seesaw circuit pool [3] and are independent from the sequences used for other experiments. These kinetic results are consistent with the results in Figure 5 in the main text and support the argument that the leak reduction in the DLD design does not rely on specific sequences. Note that the slight initial decrease in the SLD signal with input at 37 ℃ seen in Figure 5 does not appear here. This suggests that the decrease could be sequence dependent or could be an experimental artifact. The concentration of reporter was 400 nM. *F1* and *F2* were 350 nM. Input X was at 350 nM.

S3 Initial leak

Compared with the SLD design, the DLD design was also observed to decrease initial leak by a factor of about 4 (Figure 5, 6 in the main text). This decrease could be tentatively explained by the differing effects of truncations on initial leak in SLD vs DLD designs. For example as shown in Figure S2, if a fuel species in the SLD design has a truncation (i.e., the bottom strand of *F1* at the 3' end, or the top or bottom strand of *F2* at the 3' end), it is possible that the truncation site serves as a toehold and can initiate fast toehold-mediated strand displacement reactions with other fuel species. In contrast, in the DLD design, truncations of the bottom strand of *F1* or the top strand of *F2* at the 3' end would not cause similar undesired triggering. Only if the truncation occurs at the bottom strand of *F2* at the 3' end could it contribute to the initial leak. We hypothesize that this mechanism could explain the reduction in initial leak in the DLD scheme.

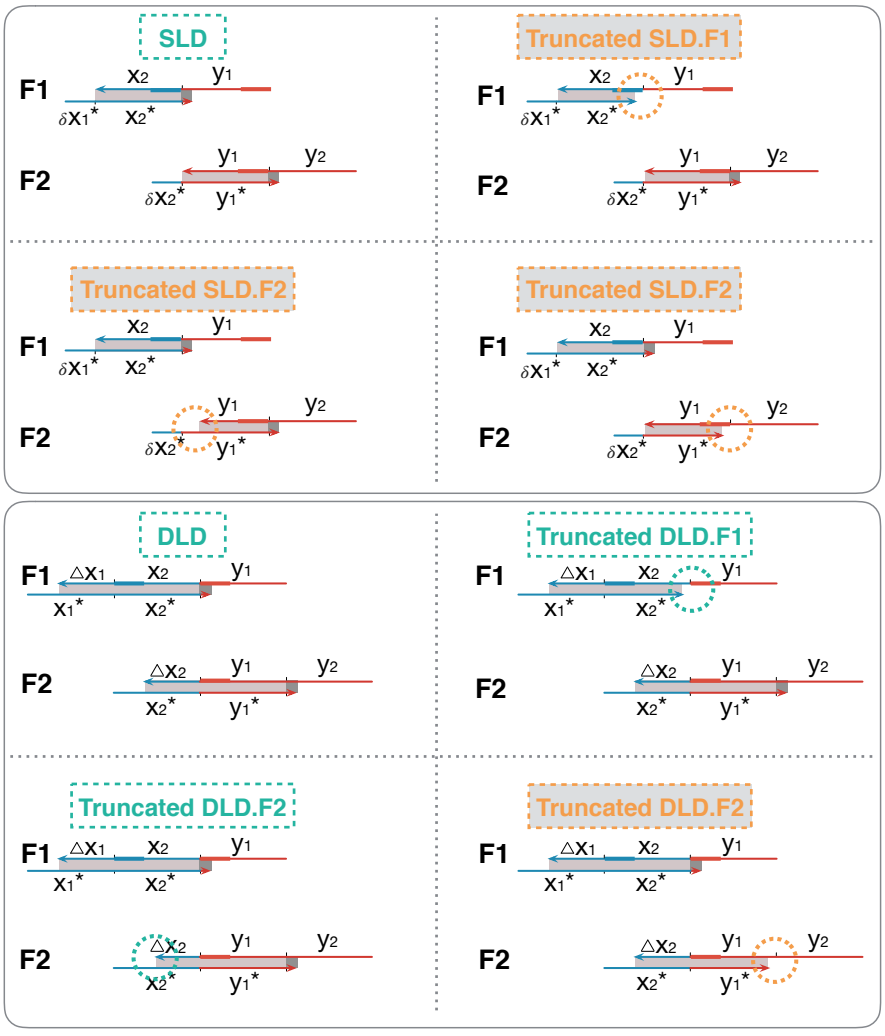

Figure S2: The schemes of SLD and DLD translators with and without truncations. The orange circles show the truncation events that could result in initial leak. The light blue circles show the truncation events that are not expected to contribute to the initial leak.

S4 Analysis of the proposed mechanism of leak in the DLD design

S4.1 Experimental and NUPACK-predicted leak concentration at equilibrium

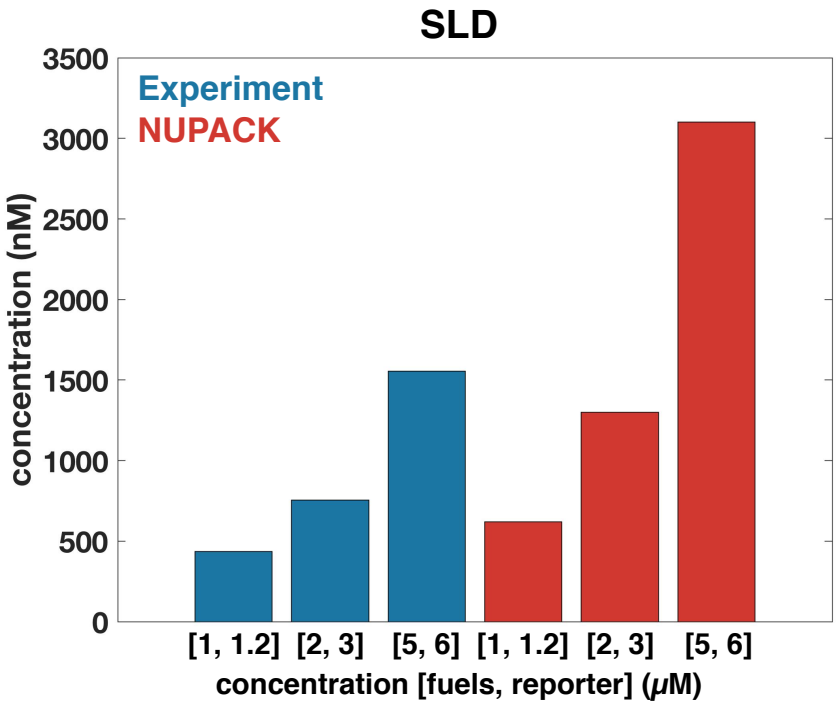

Figure S3: Concentration of the leak products in the SLD single translator system at thermodynamic equilibrium measured from annealing experiments and calculated by NUPACK [6]. The computationally predicted concentration of the leak products at equilibrium for the SLD translator was within a factor of 2 of the experimental data.

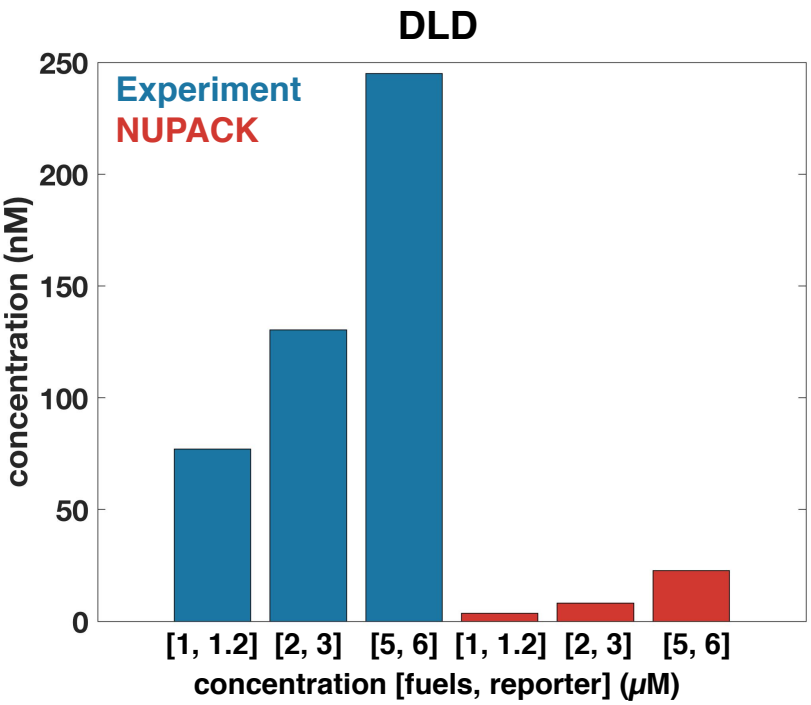

Figure S4: Concentration of the leak products in the DLD single translator system at thermodynamic equilibrium measured from annealing experiments and calculated by NUPACK. The discrepancy between the NUPACK-predicted and experimentally observed leak could be due to coaxial stacking or pseudoknotted configurations which NUPACK disregards. Note that due to the large size (4 strands) $Y_{complex}$ in the DLD design, pseudoknotts are a priori more likely than in the SLD design where all relevant complexes are small (2 strands). Both the experimentally observed and predicted leak was significantly less in the DLD design than the SLD design (Figure S3).

S4.2 Leak between reporter and *F2*

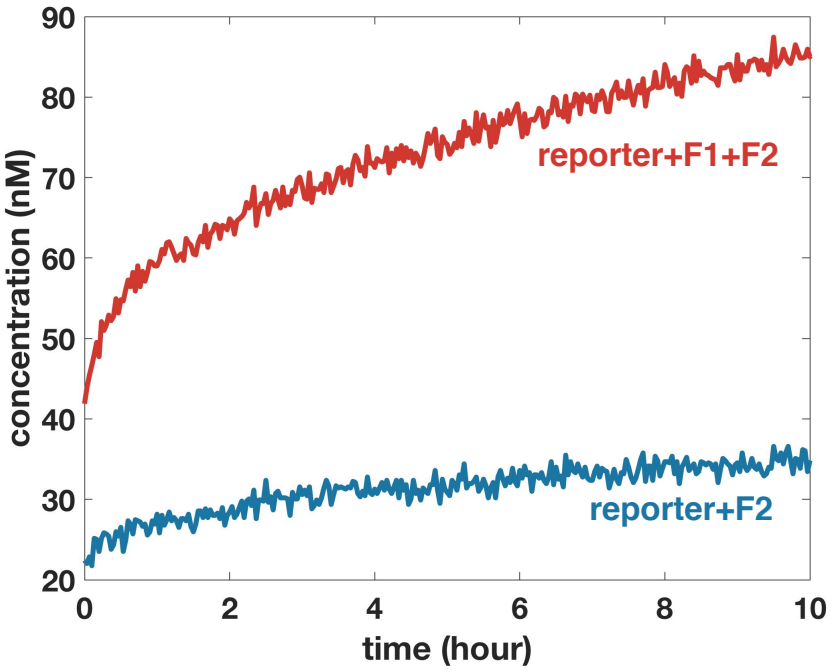

Figure S5: Leak kinetics of the DLD reporter with only fuel *F2* (blue) and with fuels *F1* and *F2* (red). The leak between the reporter and fuel *F2* only was much smaller than the leak if both fuels were present, suggesting that most of the leak involves an interaction between all three. The reporter concentration was $11\ \mu$M, and the fuel concentrations were $10\ \mu$M. Experiments were conducted at 37 ℃.

S4.3 The second phase of the DLD leak kinetics

To further analyze the kinetics of the second phase of the leak, we measured the kinetics of fuel species reacting with the reporter at different concentrations. Figure S6 shows that increasing the concentration of reporter from 6 μM to 20 μM, the leak rate of the second phase is almost the same, indicating that the rate-limiting step of the second phase does not involve the reporter. Consistent with this observation, in our model (see next section), the rate limiting step occurs prior to the reaction with the reporter, in the reconfiguration step (reaction (3)).

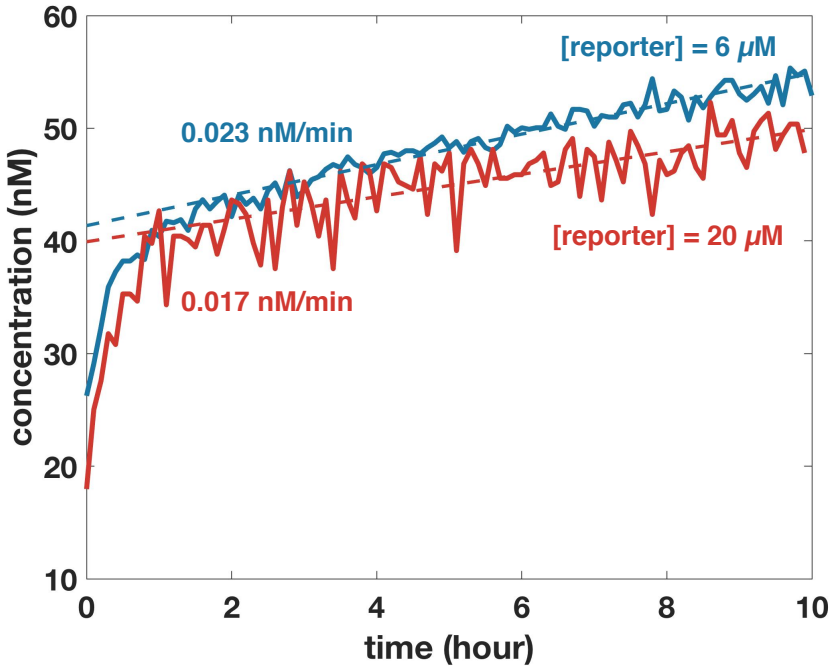

Figure S6: Kinetics of the DLD translator with a fixed concentration of the fuel species (5 μM) and different concentrations of the reporter (6 μM and 20 μM). The leak rates of the second phase are similar when the reporter concentration is increased from 6 μM to 20 μM, indicating that the rate limiting step of the second phase does not involve the reporter when the concentration of the reporter is higher or equal to 6 μM. The experiment is conducted at 37 ℃.

S4.4 Kinetic model

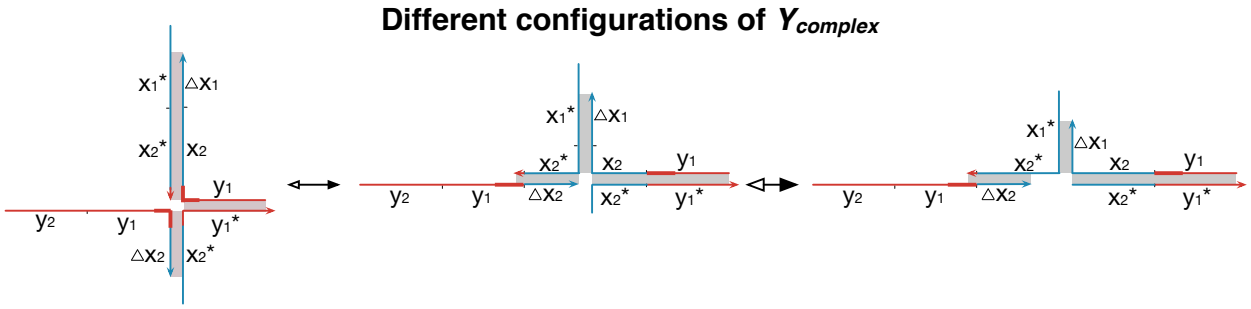

Figure S7: Different configurations of $Y_{complex}$. To reach other configurations other than the original one (left most), a 4-way branch migration step is necessary in the pathway.

In the kinetic model, the fuel species *F1* and *F2* react through toeless strand displacement and form $Y_{complex}$, which can quickly dissociate back (reaction 1) or slowly isomerize to other configurations $Y'_{complex}$ (reaction 3). Both $Y_{complex}$ and $Y'_{complex}$ can be detected by the reporter (reaction 2, 4). The species *waste*$_1$ and *waste*$_2$ emit fluorescence.

Reactions	Rate constants
(1) $F1 + F2 \underset{k_{-1}}{\overset{k_1}{\rightleftharpoons}} Y_{complex}$	$k_1 \approx 12.81$ M^{-1}s^{-1}, $k_{-1} \approx 7.09$ s^{-1}
(2) $Y_{complex} + reporter \underset{k_{-2}}{\overset{k_2}{\rightleftharpoons}} reporter_{\cdot top} + waste_1$	$k_2 \approx 3.8 \times 10^4$ M^{-1}s^{-1}, $k_{-2} \approx 2.5 \times 10^4$ M^{-1}s^{-1}
(3) $Y_{complex} \underset{k_{-3}}{\overset{k_3}{\rightleftharpoons}} Y'_{complex}$	$k_3 \approx 0.018$ s^{-1}, $k_{-3} \approx 0.0096$ s^{-1}
(4) $Y'_{complex} + reporter \underset{k_{-2}}{\overset{k_2}{\rightleftharpoons}} reporter_{\cdot top} + waste_2$	$k_2 \approx 3.8 \times 10^4$ M^{-1}s^{-1}, $k_{-2} \approx 2.5 \times 10^4$ M^{-1}s^{-1}

Table S1: Our model of the DLD leak reactions, and the best-fit rate constants.

Note that the rate constants k_3 and k_{-3} are reasonable for 4-way branch migration compared to the rate for completing a 4-way branch migration pathway that is similarly initiated from an open-loop junction, reported as 4.4×10^{-4} s^{-1} [7]. Note that the rate constants k_2 and k_{-2} were not well constrained by the model fitting.

S5 Long SLD

Recall that the SLD and DLD schemes share the same size of the single stranded region (unbound domain) in a fuel complex. This ensures that the single stranded regions potentially have equal contributions to leak in both systems. However, one may argue that the SLD design has a shorter double-stranded region in every fuel species, thus it is more favorable for the SLD design to spuriously release the output signal. Here we increased the size of the double-stranded region in the SLD scheme (calling it the *Long SLD* scheme) and let it share the same size of the bound domain as the DLD scheme (Figure S8a).

The kinetic results (Figure S8b) and the PAGE results (Figure S12, S14) confirmed that increasing the size of the bound domain (double-stranded region) in a fuel complex in the SLD scheme does not decrease leak as much as the DLD scheme. After 10 hours, the leak concentration of Long SLD (830 nM) is approximately half of the SLD translator (1570 nM), but is 15 times more than that of the DLD translator (54 nM). (Compare to Figure 6 in the main text.)

In addition, the Long SLD scheme requires longer strands than the DLD scheme, which is more expensive especially for larger systems.

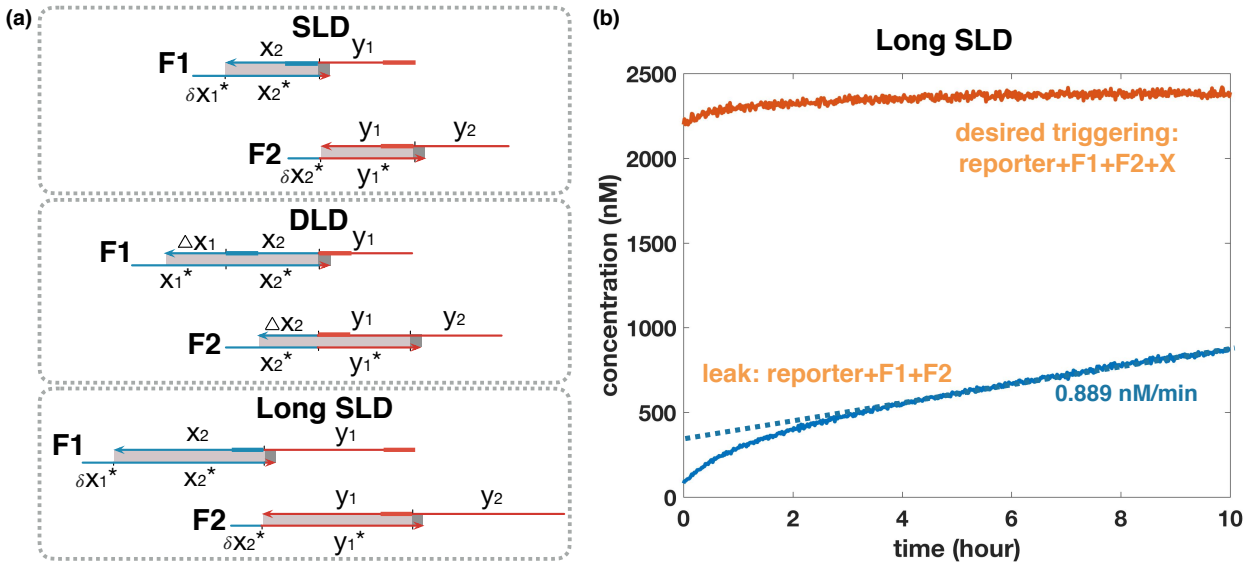

Figure S8: The Long SLD scheme. (a) Comparison between the designs of the SLD, the DLD and the Long SLD translators. The SLD and the DLD schemes share the same size of the single stranded region (unbound domain) in a fuel complex, and the Long SLD and the DLD scheme share the same size of double-stranded region (bound domain) in a fuel complex. For a fair comparison, the Long SLD and the DLD schemes also share the same reporter, so the leak rates of the two schemes are independent of the effect of the reporter. (b) Kinetics of the Long SLD translator with and without the input X at high concentration. The leak of the Long SLD translator is less than that of the SLD translator, but substantally more than in the DLD scheme. [fuels] = 5 μM, [reporter] = 6 μM, [input] = 2.5 μM. The reaction temperature is 37 ℃.

S6 TLD and NLD

S6.1 Desired triggering kinetics of the TLD design

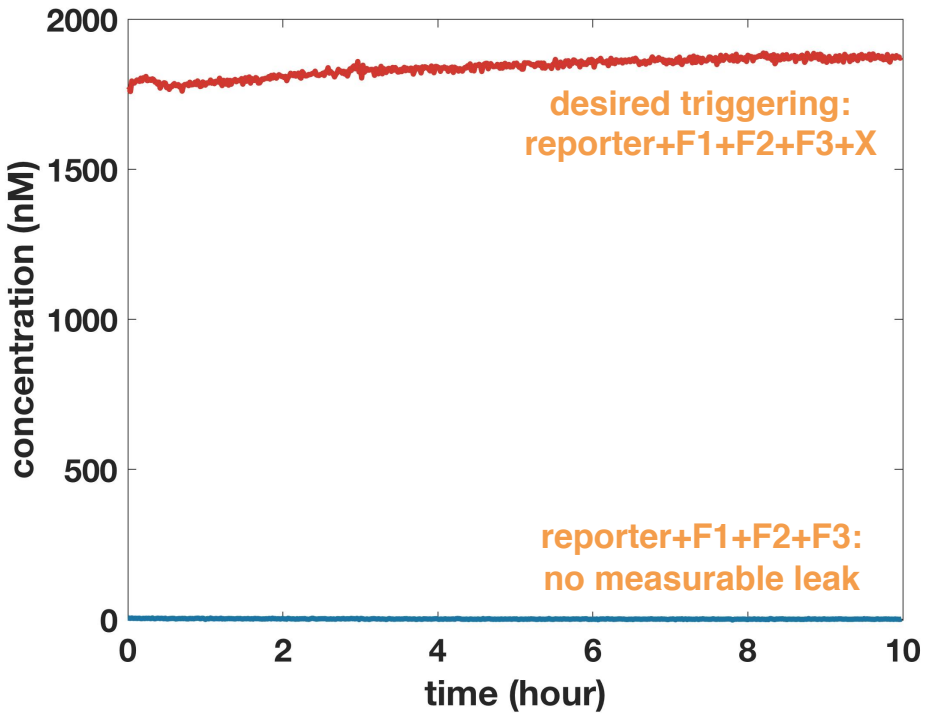

Figure S9: Kinetics of the TLD translator with and without the input X. The desired triggering signal reached about 70% at the first data point. After 10 hours, the signal reached approximately 75%. The reporter concentration was 6 μM, the fuels were at 5 μM, and the input strand was at 2.5 μM. The desired triggering signal was normalized by an internal control sample with 6 μM reporter and 2.5 μM *F3*$_{top}$ strand that was supposed to directly trigger the reporter (see Section S1.4). The experiments were conducted at 37 ℃.

S6.2 Side reaction with input of the TLD design

Here we discuss a hypothesized side reaction which may be responsible for the decrease in completion level for the TLD scheme. Instead of reacting with *F1*, the input signal strand X may skip the first layer and directly react with *F2* through binding with the toehold of *F2* and performing a 3-way branch migration step to displace domain Δx_2 and x_3 (I_1). Then I_1 invades with *F3* and displaces the domain Δx_3 (I_2), followed by a slow 4-way branch migration step (I_3). Complex I_3 then splits into two waste species after 3-way branch migration through domain y_2. The input strand X is trapped after I_2 forms.

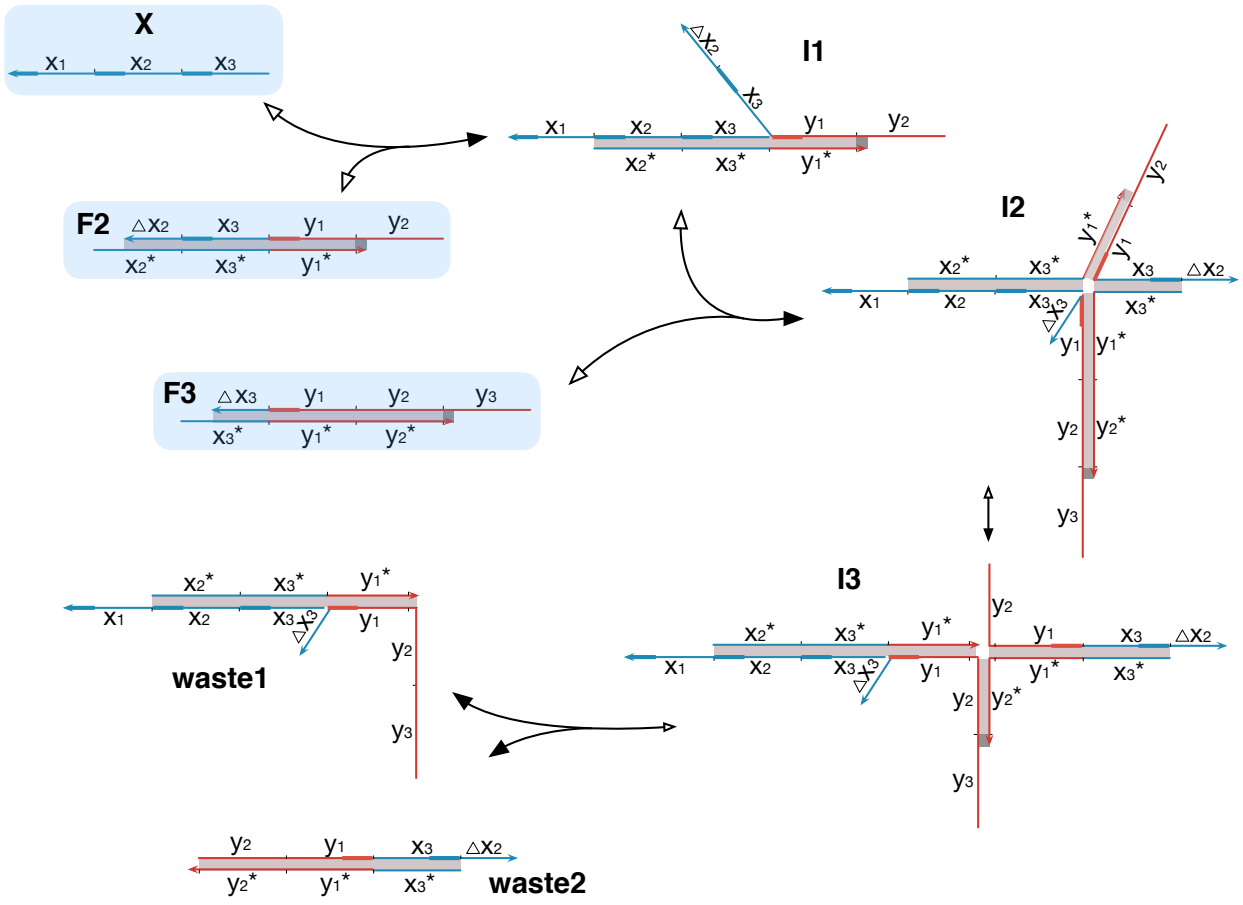

Figure S10: One possible side reaction pathway in the presence of the input signal strand.

S6.3 Leakless design with redundancy level 1

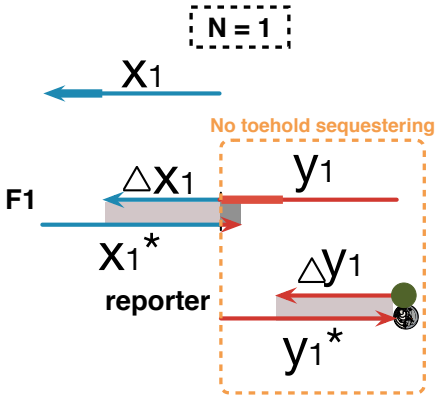

Figure S11: The leakless scheme of a translator with redundancy level $N = 1$. The toehold of domain y_1 is not effectively sequestered, thus $N = 1$ is not a valid design. Note that the leakless scheme with $N = 1$ is not the SLD scheme.

S7 PAGE visualization

In all the PAGE gels below, the right and left gels show the same gel but before (right) and after (left) staining by Sybr Gold. While Sybr Gold stains all strands and complexes, in the images on the right only the bands containing unquenched fluorophore are visible (self-fluorescence) showing leak and intended triggering.

Note that the gel results show that there exist other leak pathways that we are not explicitly mentioning in the main text. In particular, there is a substantial band (the relative leak intensity is 0.1) showing leak between *F2* and reporter (D.F2+D.reporter.bottom). Since fluorescence experiments suggest that this leak is minimal (Figure S5), we cannot readily explain this leak mechanism, which might be specific to the experimental conditions of the PAGE gel.

S7.1 SLD and DLD Gel

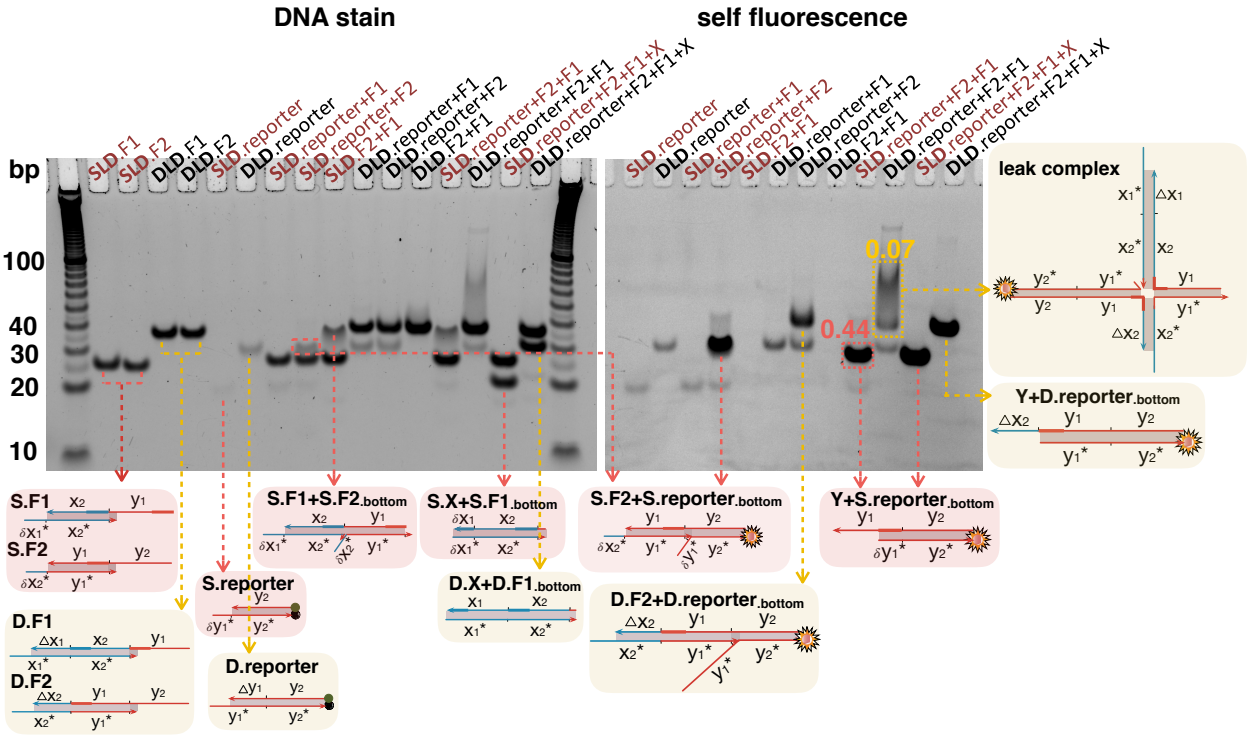

Figure S12: PAGE gel results comparing the SLD and DLD designs before (right) and after (left) Sybr Gold staining. Before Sybr Gold staining, in the lane with the DLD reporter, *F1* and *F2*, there is a wide band with self fluorescence, showing the proposed large leaked complex. The relative leak intensity of the DLD translator (0.07) is roughly 6 times smaller than that of the SLD translator (0.44).

S7.2 TLD Gel

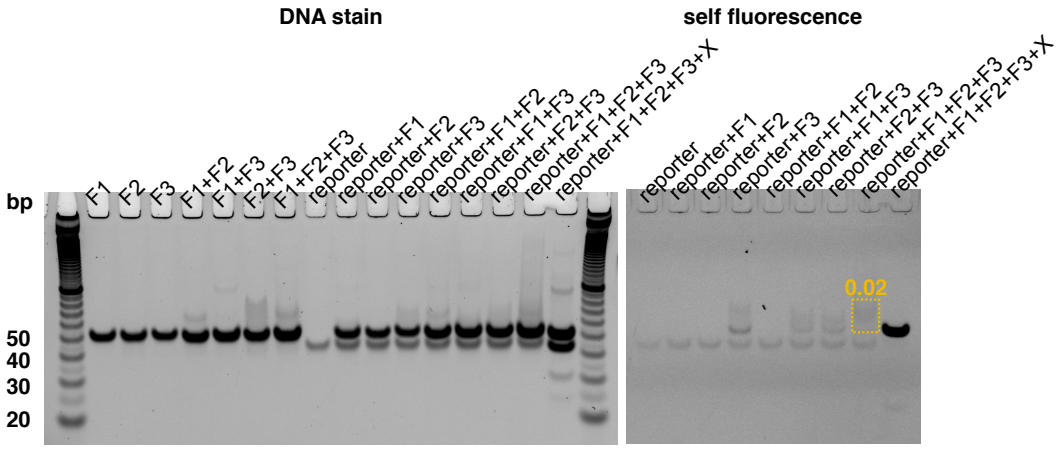

Figure S13: PAGE gel results of the TLD design before (right) and after (left) Sybr Gold staining. The relative leak intensity of the TLD translator (0.02) is smaller than that of the DLD design (0.07).

S7.3 Long SLD Gel

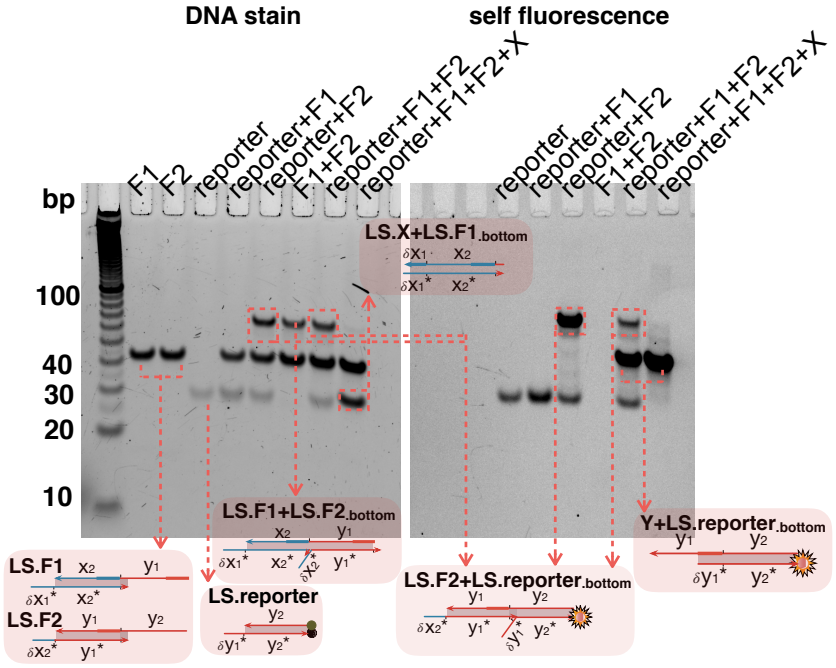

Figure S14: PAGE gel results of the Long SLD design before (right) and after (left) Sybr Gold staining. The band containing *F1* and *F2* shows apparent leaked product. The Long SLD design does not decrease leak as much as the DLD design.

S8 Cascade and *OR* circuit

S8.1 Linear translator cascade

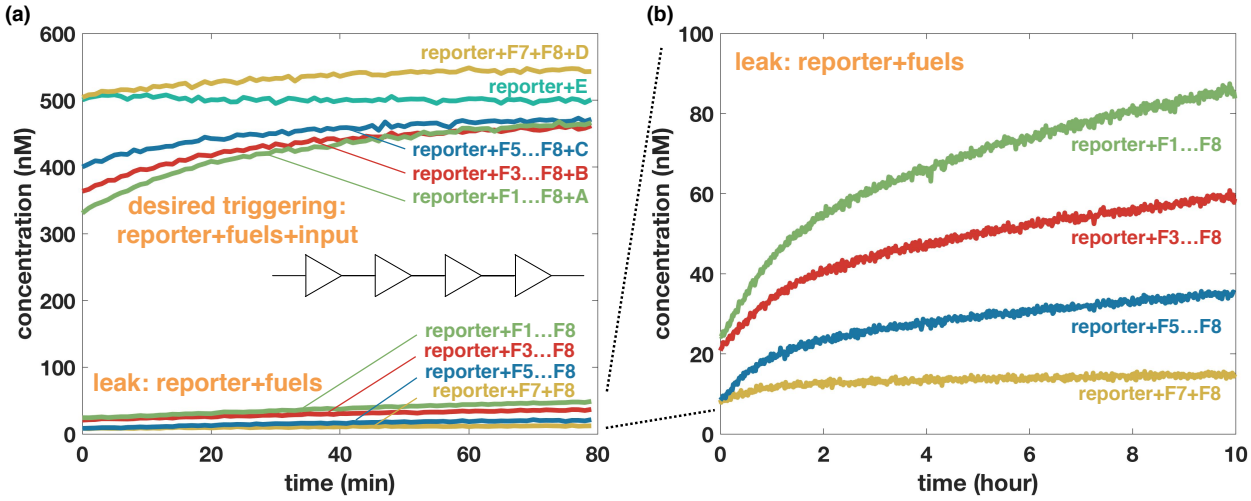

Figure S15: Linear DLD translator cascade at 37 ℃. (a,b) Kinetics of the desired triggering signal in the presence of the input, and leak signal in the absence of input. The desired triggering signals with different layers reach half-completion prior to the first measured data point. In the translator cascade, as the depth increases, leak also accumulates. The leak fraction of the longest cascade is still smaller than 9% even after 10 hours. [reporter] = [fuels] = 1 μM, [input] = 500 nM.

S8.2 *OR* circuit

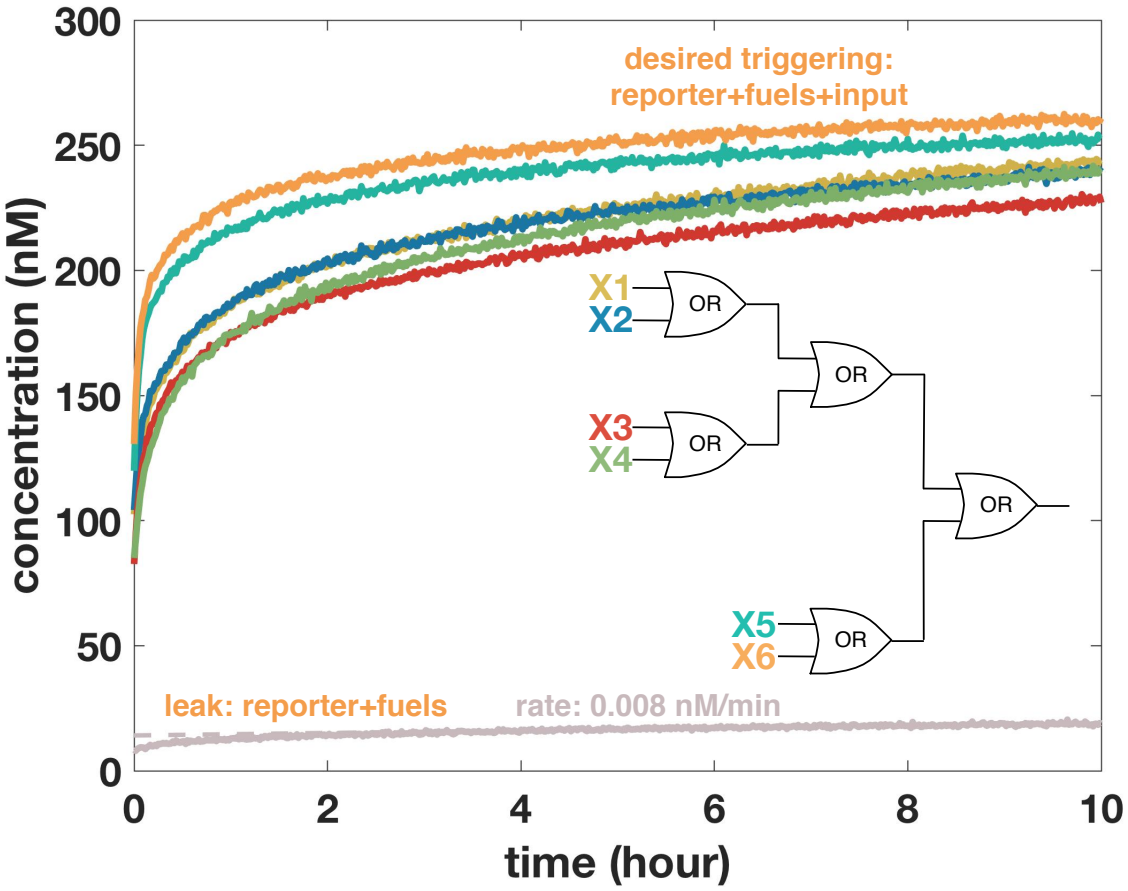

Figure S16: Kinetics of the DLD *OR* circuit with and without input signals at lower concentration. Even after 10 hours, leak is small (less than 4%). Note the contrast with Figure 9b, where the reporter was 500 nM but the fuels were 1 μM, and thus full completion as measured by the reporter (achieving 90% in 15 minutes) corresponds to half-completion of the OR cascade, whereas here the reporters and fuels had the same concentration, and thus the output fluorescence level reached completion no faster than the OR cascade itself. Consistent with this interpretation, desired triggering signals reached half-completion within 10 minutes; their slow down at longer times could have been caused by toehold occlusion [3] or substoichiometric completion levels due to imperfect fuel concentrations. [reporter] = [fuels] = 500 nM, [input] = 250 nM. Experiments were conducted at 25 ℃.

S9 Sequences

Translators

(Sequences picked from Seesaw circuit pool [3] for sequence generality experiment.)

SLD.F1top	CACTA ACATA CAACA CACAT AACAA CCACA
SLD.F1bottom	TGAGA TGTGG TTGTT ATGTG TG
SLD.F2top	CACCC TAAAA TCTCA CACTA ACATA CAACA
SLD.F2bottom	ATGTG TGTTG TATGT TAGTG TG
DLD.F1top	TAAAA TCTCA CACTA ACATA CAACA CACAT AACAA CCACA
DLD.F1bottom	TGAGA TGTGG TTGTT ATGTG TGTTG TATGT TA
DLD.F2top	ATTCC ACTCA CACCC TAAAA TCTCA CACTA ACATA CAACA
DLD.F2bottom	ATGTG TGTTG TATGT TAGTG TGAGA TTTTA GG
SLD.Rtop	/5IABkFQ/CACCC TAAAA TCTCA
SLD.Rbottom	TAGTG TGAGA TTTTA GGGTG/36-FAM/
DLD.Rtop	/5IABkFQ/ATTCC ACTCA CACCC TAAAA TCTCA
DLD.Rbottom	TAGTG TGAGA TTTTA GGGTG TGAGT GGAAT/36-FAM/
SLD.X0	CA CACAT AACAA CCACA TCTCA
DLD.X0	TA ACATA CAACA CACAT AACAA CCACA TCTCA

The sequences below were generated by the principles described in Section S1.1:

Translators

SLD.F1top	TTCCA TCACA TAACA TCCTT CTAAT CAATC
SLD.F1bottom	GTGTT GATTG ATTAG AAGGA TG
SLD.F2top	TCTCA AACCT ATACA TTCCA TCACA TAACA
SLD.F2bottom	AAGGA TGTTA TGTGA TGGAA TG
DLD.F1top	AACCT ATACA TTCCA TCACA TAACA TCCTT CTAAT CAATC
DLD.F1bottom	GTGTT GATTG ATTAG AAGGA TGTTA TGTGA TG
DLD.F2top	TCCAC TACTT TCTCA AACCT ATACA TTCCA TCACA TAACA
DLD.F2bottom	AAGGA TGTTA TGTGA TGGAA TGTAT AGGTT TG
SLD.Rtop	/5IAbRQ/TCTCA AACCT ATACA
SLD.Rbottom	TGGAA TGTAT AGGTT TGAGA/3Rox_N/
DLD.Rtop	/5IAbRQ/TCCAC TACTT TCTCA AACCT ATACA
DLD.Rbottom	TGGAA TGTAT AGGTT TGAGA AAGTA GTGGA/3Rox_N/
SLD.X0	CA TCCTT CTAAT CAATC AACAC
DLD.X0	CA TCACA TAACA TCCTT CTAAT CAATC AACAC

Long SLD

The long SLD system shares the same reporter with the DLD system.

LSLD.F1top	TTCCA ATACT CTATT ACTAT CACCA TCCTT TTACA CTTCT TAAAT CTCCT
LSLD.F1bottom	GTGTT AGGAG ATTTA AGAAG TGTAA AAGGA TG
LSLD.F2top	TCCAC TACTT TCTCA AACCT ATACA TTCCA ATACT CTATT ACTAT CACCA
LSLD.F2bottom	AAGGA TGGTG ATAGT AATAG AGTAT TGGAA TG
LSLD.X0	CATCC TTTTA CACTT CTTAA ATCTC CTAAC AC

TLD

TLD.F1top	TCACA TAACA TCCTT CTAAT CAATC AACAC ACATA TCCTC ACTCA ATACA TATAC
TLD.F1bottom	AGGAA GTATA TGTAT TGAGT GAGGA TATGT GTGTT GATTG ATTAG AA
TLD.F2top	AACCT ATACA TTCCA TCACA TAACA TCCTT CTAAT CAATC AACAC ACATA TCCTC
TLD.F2bottom	TGAGT GAGGA TATGT GTGTT GATTG ATTAG AAGGA TGTTA TGTGA TG
TLD.F3top	TCCAC TGCTT TCTCA AACCT ATACA TTCCA TCACA TAACA TCCTT CTAAT CAATC
TLD.F3bottom	GTGTT GATTG ATTAG AAGGA TGTTA TGTGA TGGAA TGTAT AGGTT TG
TLD.Rtop	/5IAbRQ/TCCAC TACTT TCTCA AACCT ATACA TTCCA TCACA TAACA
TLD.Rbottom	AAGGA TGTTA TGTGA TGGAA TGTAT AGGTT TGAGA AAGTA GTGGA/3Rox_N/
TLD.X0	CTAAT CAATC AACAC ACATA TCCTC ACTCA ATACA TATAC TTCCT

Cascade

The sequences for *F7*, *F8* and reporter are the same as the DLD translator sequences generated above by the principles described in Section S1.1.

Cascade.F1top	TTTTC AAACA ATCCA CACTA CATCT CATCA AATCA TATTC
Cascade.F1bottom	AAAGG GAATA TGATT TGATG AGATG TAGTG TG
Cascade.F2top	TCCCA TTTCA TTCAC TTTTC AAACA ATCCA CACTA CATCT
Cascade.F2bottom	TGATG AGATG TAGTG TGGAT TGTTT GAAAA GT
Cascade.F3top	ATACA TATAC TTCCT TCCCA TTTCA TTCAC TTTTC AAACA
Cascade.F3bottom	TGGAT TGTTT GAAAA GTGAA TGAAA TGGGA AG
Cascade.F4top	ACATA TCCTC ACTCA ATACA TATAC TTCCT TCCCA TTTCA
Cascade.F4bottom	GTGAA TGAAA TGGGA AGGAA GTATA TGTAT TG
Cascade.F5top	CTAAT CAATC AACAC ACATA TCCTC ACTCA ATACA TATAC
Cascade.F5bottom	AGGAA GTATA TGTAT TGAGT GAGGA TATGT GT
Cascade.F6top	TCACA TAACA TCCTT CTAAT CAATC AACAC ACATA TCCTC
Cascade.F6bottom	TGAGT GAGGA TATGT GTGTT GATTG ATTAG AA
Cascade.A	CACTA CATCT CATCA AATCA TATTC CCTTT
Cascade.B	TCCCA TTTCA TTCAC TTTTC AAACA ATCCA
Cascade.C	ACATA TCCTC ACTCA ATACA TATAC TTCCT

OR circuit

The sequences for *F1*, *F2*, *F9* and *F10* are the same as *F3*, *F4*, *F5* and *F6* in the DLD cascade above. The sequences for *F17*, *F18* and reporter are the same as the DLD translator sequences generated above by the principles described in Section S1.1.

TREE.F3top	ATACA TATAC TTCCT TCAAA CTACT ACTAC CATAC ACTCA
TREE.F3bottom	TGGTA TGAGT GTATG GTAGT AGTAG TTTGA AG
TREE.F4top	ACATA TCCTC ACTCA ATACA TATAC TTCCT TCAAA CTACT
TREE.F4bottom	GTAGT AGTAG TTTGA AGGAA GTATA TGTAT TG
TREE.F5top	CTATT CCAAC TTCTC TTAAA ACCTC TCTCT CATTT TCCCT
TREE.F5bottom	AGTAG AGGGA AAATG AGAGA GAGGT TTTAA GA
TREE.F6top	ATATT CCTCT TACCA CTATT CCAAC TTCTC TTAAA ACCTC
TREE.F6bottom	AGAGA GAGGT TTTAA GAGAA GTTGG AATAG TG
TREE.F7top	CTATT CCAAC TTCTC CATAT CTACT ATCTC CCTTC ATTAC
TREE.F7bottom	AGATG GTAAT GAAGG GAGAT AGTAG ATATG GA
TREE.F8top	ATATT CCTCT TACCA CTATT CCAAC TTCTC CATAT CTACT
TREE.F8bottom	GAGAT AGTAG ATATG GAGAA GTTGG AATAG TG
TREE.F11top	CTAAT CAATC AACAC ATATT CCTCT TACCA CTATT CCAAC
TREE.F11bottom	GAGAA GTTGG AATAG TGGTA AGAGG AATAT GT
TREE.F12top	TCACA TAACA TCCTT CTAAT CAATC AACAC ATATT CCTCT
TREE.F12bottom	TGGTA AGAGG AATAT GTGTT GATTG ATTAG AA
TREE.F13top	CCTAA TCTCT TTCAC CTTAC TTACA ACTAC AACTA ACCTC
TREE.F13bottom	GTATG GAGGT TAGTT GTAGT TGTAA GTAAG GT
TREE.F14top	TTTCC ATTCT ATCAC CCTAA TCTCT TTCAC CTTAC TTACA
TREE.F14bottom	GTAGT TGTAA GTAAG GTGAA AGAGA TTAGG GT
TREE.F15top	CCTAA TCTCT TTCAC CTAAT ATCCA CATCT AAACC TTTTC
TREE.F15bottom	GAGTA GAAAA GGTTT AGATG TGGAT ATTAG GT
TREE.F16top	TTTCC ATTCT ATCAC CCTAA TCTCT TTCAC CTAAT ATCCA
TREE.F16bottom	AGATG TGGAT ATTAG GTGAA AGAGA TTAGG GT
TREE.F19top	AACCT ATACA TTCCA TTTCC ATTCT ATCAC CCTAA TCTCT
TREE.F19bottom	GTGAA AGAGA TTAGG GTGAT AGAAT GGAAA TG
TREE.F20top	TCCAC TACTT TCTCA AACCT ATACA TTCCA TTTCC ATTCT
TREE.F20bottom	GTGAT AGAAT GGAAA TGGAA TGTAT AGGTT TG
TREE.X1	TCCCA TTTCA TTCAC TTTTC AAACA ATCCA
TREE.X2	TCAAA CTACT ACTAC CATAC ACTCA TACCA
TREE.X3	TTAAA ACCTC TCTCT CATTT TCCCT CTACT
TREE.X4	CATAT CTACT ATCTC CCTTC ATTAC CATCT
TREE.X5	CTTAC TTACA ACTAC AACTA ACCTC CATAC
TREE.X6	CTAAT ATCCA CATCT AAACC TTTTC TACTC

References

[1] D. Y. Zhang, A. J. Turberfield, B. Yurke, and E. Winfree. Engineering entropy-driven reactions and networks catalyzed by DNA. *Science*, 318(5853):1121–1125, 2007.

[2] D. Y. Zhang. Towards domain-based sequence design for DNA strand displacement reactions. In *International Workshop on DNA-Based Computers*, pages 162–175. Springer, 2010.

[3] L. Qian and E. Winfree. Scaling up digital circuit computation with DNA strand displacement cascades. *Science*, 332(6034):1196–1201, 2011.

[4] J. D. Puglisi and I. Tinoco Jr. [22] absorbance melting curves of RNA. In *Methods in enzymology*, volume 180, pages 304–325. Elsevier, 1989.

[5] A. V. Tataurov, Y. You, and R. Owczarzy. Predicting ultraviolet spectrum of single stranded and double stranded deoxyribonucleic acids. *Biophysical chemistry*, 133(1-3):66–70, 2008.

[6] J. N. Zadeh, C. D. Steenberg, J. S. Bois, B. R. Wolfe, M. B. Pierce, A. R. Khan, R. M. Dirks, and N. A. Pierce. NUPACK: analysis and design of nucleic acid systems. *Journal of computational chemistry*, 32(1):170–173, 2011.

[7] N. L. Dabby. *Synthetic molecular machines for active self-assembly: prototype algorithms, designs, and experimental study*. PhD thesis, California Institute of Technology, 2013.